Adsorption (2019) 25:429–442
https://doi.org/10.1007/s10450-019-00022-8

Synthesis and characterization of mesoporous polymeric microspheres of methacrylic derivatives of aromatic thiols

K. Fila[1] · Y. Bolbukh[2] · M. Goliszek[1] · B. Podkościelna[1] · M. Gargol[1] · B. Gawdzik[1]

Received: 29 October 2018 / Revised: 14 January 2019 / Accepted: 25 January 2019 / Published online: 14 February 2019

Abstract
The paper presents the synthesis and characterization of mesoporous microspheres of derivatives of three aromatic thiols: S-phenyl 2-methylprop-2-enethioate (PSM), S,S′-thiodi-4,1-phenylenebis(thiomethacrylate) (DMSPS), and bis[4(2-hydroxy-3-methacryloyloxypropoxy)phenyl]sulfide (BES.DM) with divinylbenzene (DVB). The microspheres were obtained by the emulsion-suspension polymerization procedure. The chemical and porous structure, morphology, and properties of the microspheres were analyzed by attenuated total reflection-Fourier transform infrared (ATR/FT-IR) spectroscopy, low-temperature nitrogen adsorption data, optical microscope MORPHOLOGI G3, differential scanning calorimetry (DSC), and wavelength dispersive X-ray fluorescence (WD-XRF). Moreover, studies on the Pb(II) ions sorption process were carried out on the above mentioned compounds. The sorption kinetics and mechanism were described by the pseudo-first order, pseudo-second order, and intraparticle diffusion models. The sorption equilibria were described by the Langmuir and Freundlich isotherms. The PSM-DVB, DMSPS-DVB, and BES.DM-DVB microspheres exhibit high thermal resistance and good adsorption properties of Pb(II) ions. The best adsorption properties for the examined microspheres were obtained at pH 5. The highest monolayer adsorption capacity determined by Langmuir isotherm was obtained for the DMSPS-DVB microspheres and was equal to 22.54 mg/g. The preliminary studies show that the synthesized microspheres can be used as heavy metal ion sorbents from aqueous solutions.

Keywords Mesoporous microspheres · Methacrylate derivatives · Thiols · Thermal properties · Heavy metal sorbents

1 Introduction

Currently water pollution with heavy metal ions is a global environmental problem. It is common knowledge that one of the basic human needs in a properly functioning society is access to fresh and clean water. As a consequence, the regulations concerning heavy metal emissions into the aqueous environment as well as greater requirements for minimizing their occurrence in water become more and more urgent. A very important and still not fully solved problem is the effective removal of heavy metal ions from aqueous solutions (Carlos and Einschlag 2013; Giraldo et al. 2013; Goon et al. 2010; Hua et al. 2012; Liu et al. 2008; Amin and Khodabakshi 2010).

There are conventional methods for the removal of heavy metal ions from water and wastewater such as coagulation, chemical precipitation, solvent extraction, reverse osmosis, ion exchange, or electrolysis. Despite many advantages, these methods also have disadvantages, including, for example, small efficiency in the case of low concentrations, generation of toxic wastes, or high costs. In the protection of the aquatic environment, more attention is paid to the development of new, economical, and effective materials (Carlos and Einschlag 2013; Neyaz et al. 2013).

The materials such as metal nanoparticles, carbon nanotubes, dendrimers, or zeolites have a number of characteristic physicochemical properties, so they are considered as very efficient and convenient sorbents. Materials in the form of micro- and nanoparticles deserve a lot of attention. They are characterized by numerous unique properties, including low toxicity, chemical inertness, or biocompatibility.

✉ K. Fila
karolina.fila@poczta.umcs.lublin.pl

[1] Department of Polymer Chemistry, Faculty of Chemistry, Maria Curie-Skłodowska University, M. Curie-Skłodowska Sq. 5, 20-031 Lublin, Poland

[2] Chuiko Institute of Surface Chemistry of National Academy of Sciences of Ukraine, 17 General Naumov Str, 03164 Kyiv, Ukraine

Therefore, they are a great potential in the field of water treatment from various impurities. In addition, micro- and nanoparticles are very efficient in heavy metal separation, high reactivity to removed ions, and rapid sorption kinetics. These properties are due to their very small sizes, nanopores occurrence, and large surface area (Savage and Diallo 2005; Petcharoen and Sirivat 2012; Huang et al. 2011).

An effective sorbent with both high capacity and fast rate adsorption should have two principal characteristics: functional groups and a large surface area. Unfortunately, most current inorganic sorbents rarely have both at the same time. Carbon nanomaterials have large surface area but no adsorbing functional groups. On the contrary, some organic polymers, e.g. polyphenylenediamine, containing a large number of functional groups (amino groups) can effectively adsorb heavy metal ions, whereas their small specific area and low adsorption rate limit their application.

As a result, new sorbents with both functional groups and large surface area are still required. In addition, it is crucial to develop affordable and environmentally friendly nanomaterials. Therefore, with the development of nanotechnology, the use of new effective adsorption materials is essential and will continue indefinitely, the future of new functional materials in the removal of heavy metal ions in waste water treatment is quite clear (Huang et al. 2011; Pan et al. 2009; Zhao et al. 2011; Podkościelna 2013; Podkościelna et al. 2016).

Recently, much attention has been paid to polymers containing thiol groups to be used as selective sorbents for removal of heavy metal ions and other elements in the water and wastewater treatment processes. The thiol group is an excellent ligand due to its strong affinity for various heavy metal ions especially for mercury ions (Podkościelna et al. 2016; Podkościelna and Kołodyńska 2013). Several routes for incorporating thiols into different filtration substrates, such as ceramic, biomagnetic particles, poly(methyl methacrylate), silica, alumina, and carbon nanotubes have been studied (Ho 1975; He et al. 2012; Zhang et al. 2012; Lee et al. 2013; Yantasee et al. 2007). For instance, the surfaces of Zn-doped biomagnetite nanostructured particles were functionalized with (3-mercaptopropyl)trimethoxysilane (MPTMS) and used as a high-capacity and collectable adsorbent for the removal of Hg(II) from water (He et al. 2012). The efficacy of thiol-functionalized alumina for removing arsenic was evaluated (Hao et al. 2009) and it was found that the thiol groups were able to remove both As(III) and As(V) ions. Removal of heavy metal ions using the thiol-functionalized mesoporous silica was investigated (Li et al. 2011) and it was demonstrated that more than 90% removal rate can be achieved in the case of Hg(II), Pb(II), Ag(I), and Cu(II) ions.

In this paper sulfur-containing monomers were used to obtain effective ion exchangers by introducing them directly into the polymer matrix. The possibility of using the prepared polymeric microspheres methacrylic derivatives of aromatic thiols for removal of key heavy metal ion- Pb(II) from the contaminated water was also investigated.

2 Experimental

2.1 Materials

Decan-1-ol and the sodium salt of bis(2-ethylhexyl)sulphosuccinate (DAC, BP) were supplied by Fluka AG (Buchs, Switzerland). α,α′-Azoisobisbutyronitrile (AIBN) and divinylbenzene (DVB) were obtained from Merck (Darmstadt, Germany). S,S′-thiodi-4,1-phenylenebis(thiomethacrylate) (DMSPS) and lead nitrate ($Pb(NO_3)_2$) were purchased from Sigma-Aldrich (Sweden). Toluene, acetone, methanol, hydrochloric acid, and sodium hydroxide were from Avantor Performance Materials (Gliwice, Poland). S-phenyl 2-methylprop-2-enethioate (PSM) and bis[4(2-hydroxy-3-methacryloyloxypropoxy)phenyl]sulphide (BES.DM) were obtained by the procedures described in our previous papers (Fila et al. 2018; Podkościelna et al. 2009; Grochowicz and Gawdzik 2013). All chemicals were used as received.

2.2 Methods

2.2.1 Synthesis of sulfur microspheres with divinylbenzene

Copolymerization with DVB was performed in the aqueous medium. Figure 1 shows the chemical structure of the monomers used for copolymerization. In the first stage 150 mL of distilled water and 1.40 g of bis(2-ethylhexyl)sulfosuccinate sodium salt (as a surfactant) were stirred for 0.5 h at 80 °C in a three necked round-bottom flask fitted with a stirrer, a dropping funnel, and a thermometer. Then the solution containing 8.70 g of the PSM, 5 g of the DVB, 0.21 g of the AIBN (as an initiator), and the mixture of pore-forming diluents (toluene and decan-1-ol) were added while stirring to the aqueous medium. Copolymerization was performed for 18 h at 80 °C. The obtained copolymers in the form of porous microspheres were washed with distilled water, filtered off, dried, and extracted in a Soxhlet apparatus with boiling acetone and methanol. After drying the microspheres were fractionated with sieves. The DMSPS-DVB microspheres were obtained in the same way. The synthesis of BES.DM-DVB microspheres was made according to the Podkościelna et al. procedure (2009). In Table 1 the experimental parameters of the syntheses are presented.

2.2.2 Characterization of the samples

The attenuated total reflection–Fourier transform infrared (ATR/FT-IR) spectra were obtained with a FTIR TENSOR

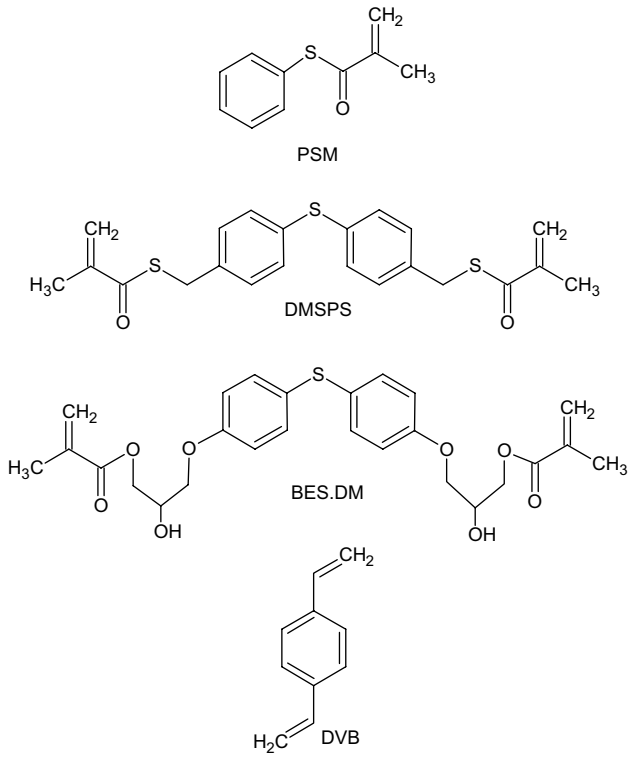

Fig. 1 Chemical structure of the monomers used for copolymerization

27 (Bruker, Germany) spectrophotometer. They were recorded from 4000 to 600 cm^{-1} averaging 32 scans with a resolution of 4 cm^{-1}.

Differential scanning calorimetry (DSC) experiments were performed with a Netzsch 204 calorimeter (Germany). All DSC measurements were taken in the aluminium pans with the pierced lid (mass of 40 ± 1 mg). Empty aluminium crucible was applied as a reference. Sample masses of about 10 mg were used. The sample pan was placed in the calorimeter at ~25 °C. Dynamic scans were made at a heating rate of 10 K/min in the temperature range 20–500 °C. The decomposition temperature (T_{peak}), glass transition temperature (T_g), and enthalpy of decomposition (ΔH_d) were determined.

The porous structure of copolymers was characterized by nitrogen adsorption at 77 K using an ASAP 2405 adsorption analyzer (Micrometrics Inc., USA). Before the analysis the copolymers were outgassed at 150 °C for 2 h. Specific surface areas were calculated by the Brunauer–Emmett–Teller (BET) method, assuming that the area of a single nitrogen molecule in the adsorbed state is 16.2 Å. Pore volumes and pore size distributions were determined by the Barrett-Joyner-Halenda (BJH) method.

Morphology of the obtained microspheres was confirmed using the optical microscope MORPHOLOGI G3 Malvern. A small drop of microspheres suspension was placed on a clean glass slide examined under the microscope.

The swellability coefficients (B) were determined by equilibrium swelling in acetone, methanol, acetonitrile, tetrahydrofuran (THF), toluene, chloroform, and distilled water using the centrifugation method (Tuncel et al. 1996; Kesenci et al. 1996). B is expressed as:

$$B = \frac{V_s - V_d}{V_d} \times 100\% \quad (1)$$

where V_s is the volume of the copolymer after swelling, V_d is the volume of the dry copolymer.

The sulfur content in the tested samples (PSM-DVB, DMSPS-DVB, and BES.DM-DVB) was examined using the WD-XRF method. The tests were carried out on the X-Ray Fluorescence Spectrometer Axios mAX (PANalytical—The Netherlands). The samples for measurement were prepared from a homogeneous material in the form of solid material, i.e. compressed tablets. In the Axios spectrometer, the exciting radiation is produced in an X-ray tube with a Rhodium anode (Rh) with a power of 4 kW. Detection of radiation takes place using two X-ray detectors: a flow detector and a scintillation detector. The XRF method is based on the fact that each element contained in the analyzed sample, as a result of X-ray excitation, emits its characteristic spectrum that is the basis for qualitative and quantitative analyses.

2.2.3 Batch adsorption studies

The uptake of heavy metal ions: Pb(II) by PSM-DVB, DMSPS-DVB, and BES.DM-DVB microspheres from water containing single metal ions was studied in the batch

Table 1 Experimental parameters of the syntheses of the microspheres

Sample	Monomers (g)				Pore-forming diluents (mL)		Initiator (g)
	PSM	DMSPS	BES.DM	DVB	Toluene	Decan-1-ol	AIBN
PSM-DVB	8.70	–	–	5	5	5	0.21
DMSPS-DVB	–	6	–	2.02	6	6	0.12
BES.DM-DVB	–	–	10	2.60	5	5	0.18

sorption-equilibrium experiments. The effects of pH, phase contact time, and the initial concentration of heavy metal ion on the sorption rate and capacity were investigated. Metal ions solutions of Pb(II) of appropriate concentrations were prepared from reagent grade $Pb(NO_3)_2$, using distilled water. The 0.1 mol/L hydrochloric acid and sodium hydroxide solutions were used for pH adjustment.

Sorption studies were carried out in a laboratory shaker (358, Elpin+, Poland). The pH-meter (PHM82 Radiometer, Copenhagen) was used for pH measurement of metal ions solutions. Concentrations of Pb(II) ions in the filtrate were measured by a Flame Atomic Absorption Spectrometer (FAAS, SpectrAA, 240FS, Varian).

The effect of pH on the sorption effectiveness of PSM-DVB, DMSPS-DVB, and BES.DM-DVB with Pb(II) ions was investigated in the pH range from 1 to 5 at 298 K. The initial concentration of Pb(II) ions was 50 mg/L. Agitation time was equal 360 min.

The effect of contact time on Pb(II) ions sorption was studied in the chosen time: 1, 3, 5, 7, 10, 30, 60, 120, 240, 360 min at a selected pH. The initial concentration was 50 mg/L for Pb(II) ions.

The effect of the initial Pb(II) ions concentration on the sorption was measured at pH 5. The concentrations of Pb(II) ions in the adsorption medium were equal 25, 50, 100, 150, 200, 300, and 500 mg/L. Measurement was carried out for 360 min at 298 K.

The sorption of Pb(II) ions on the polymeric microspheres was investigated by batch operation as a function of pH, contact time, and initial concentrations of heavy metal ions. Fifty milligrams (0.05 g) of PSM-DVB, DMSPS-DVB, and BES.DM-DVB microspheres were shaken in 250 mL Erlenmayer flasks with 10 mL of metal ion-bearing solutions at fixed time intervals on a laboratory shaker at 180 rpm with the desired pH and room temperature. Then they were filtered and the concentration of Pb(II) ions in the filtrate was determined.

Sorption parameters such as amount of the metal ions adsorbed per gram of polymer samples, q_t (mg/g) (2) and sorption percentage, %S (3) were calculated using following formulas:

$$q_t = \left(C_0 - C_t\right) \times \frac{V}{m} \tag{2}$$

$$\%S = \frac{C_0 - C_t}{C_0} \times 100\% \tag{3}$$

where: C_0 is the initial concentration of Pb(II) ions in the solution (mg/L), C_t is the concentration of Pb(II) ions after time t (mg/L), V is the volume of initial solution (mL), m is the mass of polymer samples (g).

2.2.4 Adsorption kinetic and isotherm studies

The adsorption kinetic studies were performed to describe the adsorption mechanism of Pb(II) ions on three microsphere materials. To that end, the following kinetic equations were used: the pseudo-first order (4), pseudo-second order (5), and Weber and Morris intraparticle diffusion (6). Experimental data were calculated using following equations:

$$\log(q_e - q_t) = \log(q_e) - \frac{k_1 t}{2.303} \tag{4}$$

$$\frac{t}{q_t} = \frac{1}{k_2 q_e^2} + \frac{1}{q_e} t \tag{5}$$

$$q_t = k_i t^{0.5} + C \tag{6}$$

where: q_e and q_t is the amount of adsorbed Pb(II) ions at equilibrium and at time t (mg/g), k_1 is the rate constant of the pseudo-first order equation (1/min), k_2 is the rate constant of the pseudo-second order equation (g/mg min), k_i is the intraparticle diffusion coefficient (mg/g $\text{min}^{0.5}$), and C is the constant.

In this study, the Langmuir and Freundlich isotherm models were used to describe equilibrium adsorption (Langmuir 1916; Freundlich 1906). These models were commonly used. The linear form of the Langmuir model is given by:

$$\frac{C_e}{q_e} = \frac{1}{q_0 K_L} + \frac{C_e}{q_0} \tag{7}$$

and the Freundlich isotherm model is presented as:

$$\log q_e = \log K_F + \frac{1}{n} \log C_e \tag{8}$$

where: q_0 is the monolayer sorption capacity (mg/g), K_L is the Langmuir constant (L/mg), K_F (mg/g), and n are the Freundlich constants.

3 Results and discussions

3.1 ATR/FT-IR studies

The ATR/FT-IR analysis confirms the correct course of the copolymerization reaction. The results of the analysis are listed in Table 2. Figure 2 shows the ATR/FT-IR spectra of the obtained copolymers. In the spectra of these copolymers, C–H stretching vibrations of aliphatic methyl groups are observed at about 2930 cm^{-1}. In the spectral region around 3020 cm^{-1} the C–H aromatic stretch vibrations can be noticed. The strong peaks at ~1700 cm^{-1} correspond to the carbonyl group. The absorption peaks from 1500 cm^{-1} to 1600 cm^{-1} can be attributed to the C–C aromatic ring

Table 2 The results of ATR/FT-IR analysis of the copolymers

Copolymer	Wavenumber (cm^{-1})							
	ν –OH	ν C_{Ar}–H	ν $–CH_3$	ν C=O	ν C–C_{Ar}	δ –CH	ν O–C=O	δ C_{Ar}–H
PSM-DVB	–	3024	2928	1727	1598	1449 1370	–	1104 992
DMSPS-DVB	–	3025	2929	1689	1576	1468 1383	–	1013 919
BES.DM-DVB	3489	3026	2933	1721	1590	1458	1168 1234	1038 942

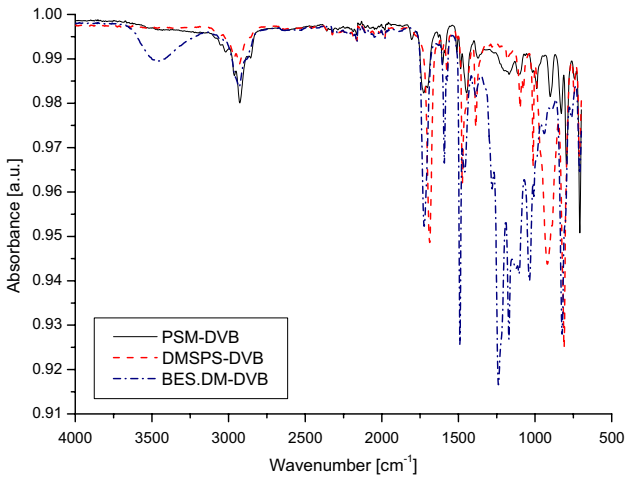

Fig. 2 ATR/FT-IR spectra of three copolymers of PSM-DVB, DMSPS-DVB, and BES.DM-DVB

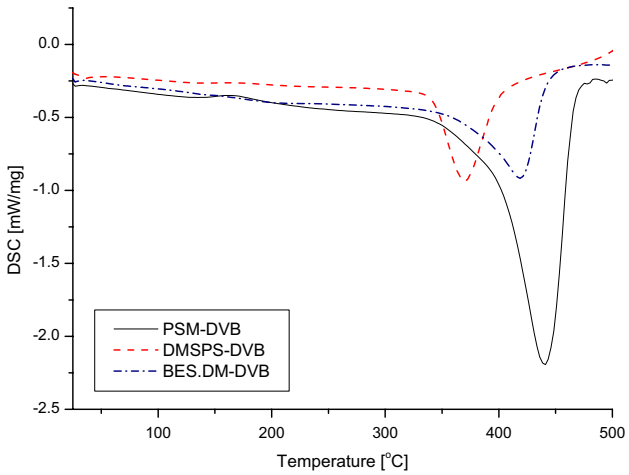

Fig. 3 DSC curves of PSM-DVB, DMSPS-DVB, and BES.DM-DVB

stretching vibrations. The peaks from 1370 cm^{-1} to 1487 cm^{-1} are due to the in-plane and out-of-plane aliphatic C–H bending. The absorption bands at 1013–1104 cm^{-1} and 919–992 cm^{-1} are assigned to the in-plane and out-of-plane rings C–H bending, respectively. In addition, on the BES.DM-DVB spectrum (Sample 3), the hydroxyl group (–OH) gives a shape signal at 3489 cm^{-1} and also the ester group occurs at 1234 cm^{-1}.

3.2 Thermal properties

Thermal properties of the obtained copolymers were studied by means of DSC analysis. The DSC curves of mesoporous copolymers are presented in Fig. 3. In addition, the characteristic temperatures: T_g, T_{peak}, and the enthalpy of decomposition (ΔH_d) are given in Table 3. The data in Table 3 indicate that the thermal properties of the copolymers containing DVB are significantly different. On the curves, only one endothermic effect connected with the thermal degradation is visible at 441 °C for the PSM-DVB copolymer (Sample 1), 419 °C for the DMSPS-DVB copolymer (Sample 2), and at 372 °C for the BES.DM-DVB copolymer (Sample 3), detected in T_{peak}. The values of the enthalpy

Table 3 DSC data for the studied copolymers

Sample	T_g (°C)	T_{peak} (°C)	ΔH_d (J/g)
PSM-DVB	156	441	571.6
DMSPS-DVB	154	419	202.4
BES.DM-DVB	152	372	146.7

of decomposition (ΔH_d) are in the range 146.7–571.6 J/g depending on the type of monomer used in the copolymerization reaction. The highest value of decomposition enthalpy is exhibited by the PSM-DVB copolymer (571.6 J/g) and the lowest by the BES.DM-DVB copolymer (146.7 J/g). The copolymers of DVB have similar T_g values ranging from 152 to 156 °C. The analysis of the DSC data leads to the conclusion that the synthesized copolymers are characterized by good thermal resistance.

3.3 Porous structure characterization

A well-developed surface area and the presence of micro- and mesopores are very important for effective sorption processes. For this reason, the study of the synthesis of high-porosity material is a very crucial issue. Such parameters as

specific surface areas, pore volumes, and average pore diameters were determined by the method of nitrogen adsorption on the surface of the studied microspheres in a dry state. Table 4 presents the characterization of porous structure of the obtained microspheres.

Figure 4 shows the adsorption–desorption isotherms of nitrogen for polymeric microspheres from three types of copolymers. The type of isotherm is common for the all samples, namely they are characterized by the fourth type according to the Brunauer's classification (a certain superposition of isotherms of II and IV types of the IUPAC classification without plateau adsorption at high p/po), but the type of the hysteresis loop is different (Sing 1982; Gregg and Sing 1991; Donohue and Aranovich 1998a, b; Condon 2006; Thommes et al. 2015). It may be due to different pores shape and size.

The reversible Type II isotherm is the normal form of isotherm obtained with a non-porous or macroporous adsorbent (The reversible Type II isotherm is characteristic of non-porous or macroporous adsorbents). The Type II isotherm represents unrestricted monolayer-multilayer adsorption. Characteristic features of the Type IV isotherm are its hysteresis loop, which is associated with capillary condensation taking place in mesopores, and the limiting uptake over a range of high p/p° that was not detected for the samples under study. The initial part of the Type IV isotherm is attributed to the monolayer-multilayer adsorption since it follows the same path as the corresponding part of the Type II isotherm obtained with the given adsorptive on the same surface area of the adsorbent in the non—porous form. For Sample 1 (PSM-DVB) the beginning of the almost linear middle section of the isotherm at $p/p_0 = 0.08$ (Point B) is often taken as the point of monolayer coverage completing and beginning of the multilayer adsorption (Fig. 4a). The hysteresis loop (Sample 1) can correspond to both Type H-1 and Type H-2. Type H-1 is narrow, the adsorption and desorption branches are almost vertical and nearly parallel. This Type (H-1) has been associated with porous materials made from agglomerates or compacts of approximately uniform spheres and having a narrow pore-size distribution. On the other hand, the Type H-2 loop is broad with the desorption branch being much steeper than the adsorption branch. Type H-2 can be found in many porous adsorbents and is believed to occur in the systems where the distribution of pore sizes and shapes is wide. It is believed that this kind of loop results when there is a difference in mechanism between the condensation and evaporation and that occurs in the pores with narrow necks and wide bodies or when the

Table 4 Parameters of the porous structures of the studied microspheres

Sample	Single point at p/p° = 0.251025213		BET	t-Plot			BJH		
	S (m^2/g)	V_{pore} (cm^3/g)	S (m^2/g)	S_{micro} (m^2/g)	$S_{external}$ (m^2/g)	V_{pore} (cm^3/g)	S (m^2/g)	V_{pore} (cm^3/g)	Pore size (nm)
PSM-DVB	493.18	1.107	517.96	–	541.70	−0.018	440.78	1.050	9.50
DMSPS-DVB	196.05	0.419	203.55	18.32	185.23	0.006	133.51	0.358	10.72
BES.DM-DVB	105.74	0.558	112.01	–	121.47	−0.007	119.91	0.561	18.71

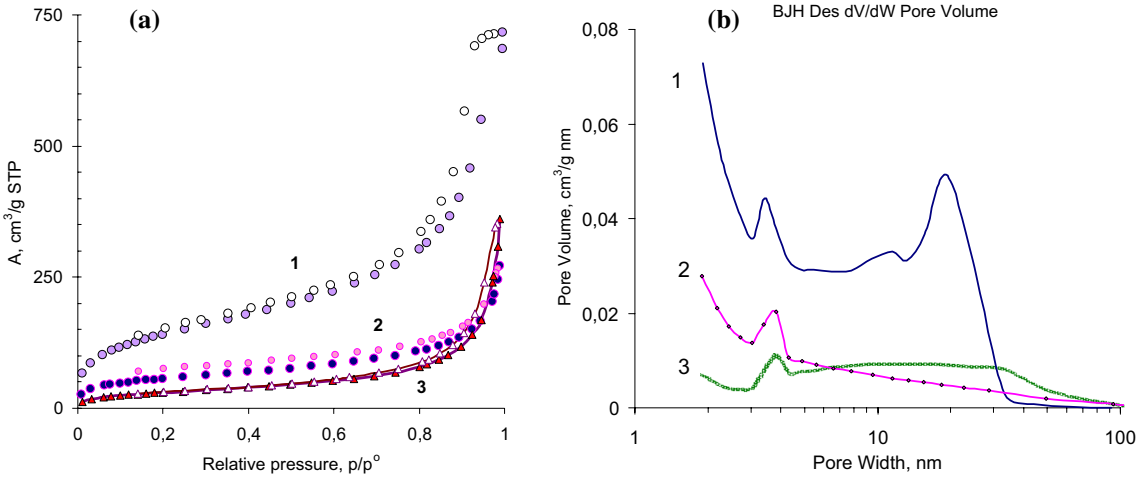

Fig. 4 Adsorption–desorption isotherms of nitrogen at 77 K (**a**) and pore size distribution (**b**) for the PSM-DVB (1), DMSPS-DVB (2), and BES.DM-DVB (3) microspheres

porous material has an interconnected pore network of different sizes and shapes (Sangwichien et al. 2002).

For Sample 1, the greatest specific surface area (S) was noted with a relatively narrow pore size distribution of the bimodal character and with the extrema at 19.2 and 9.4 nm. The weakly expressed extrema are observed at about 22 nm on the curve of Sample 2, and for Sample 3 - at 9.4 and 24.4 nm (Fig. 4b). The wide pore size distribution indicates in the samples a mixed content of predominantly macro and micropores. In contrast to the samples under discussion, Sample 1 is mesoporous with a high specific surface area - S_{BJH} is 440 m^2/g and the middle pore size D is 9.50 nm (Table 4). The Type VI isotherm is typical of mesoporous materials with strongly adsorbing surfaces whereas the Type II—is non-porous and macroporous materials with strong adsorbate–adsorbent interactions (Rouquerol et al. 1999). In the case of the obtained isotherm related to the above-mentioned types, applying the t-plot analysis determined, was useless the intercept of the t-plot appears in the negative side of the scale. This can be regarded as the evidence of the absence of micropores in Sample 1. The specific surface area calculated by the BET method (S_{BET}) was 517 m^2/g, which is significantly higher than S_{BJH}, but it can serve as the best description (reliability) since the BET model correlates well with the Type IV isotherms and is the most suitable one for mesoporous material description.

The isotherm of Sample 2 also corresponds to Type IV, however, the hysteresis loop belongs to the Type H-4. The type H-4 loop does not terminate in a plateau at high p/p_0 and therefore the limiting desorption boundary curve is more difficult to establish. The characteristic features of some types of loops are associated with certain well-defined pores structures. The Type H-4 loop is nearly horizontal and parallel over a wide range of p/p_o and is associated with the narrow slit-like pores mainly in the micropore range (Sangwichien et al. 2002; Rouquerol et al. 1999).

The beginning of the almost linear middle section of the isotherm, which is taken as a point of monolayer coverage completing, for Sample 2 is observed at $p/p_0 = 0.11$ (Fig. 4a). The specific surface area (S_{BET} and S_{BJH}) of Sample 2 is much lower than that of Sample 1, but the average pore diameter calculated from the BJH equation differs insignificantly: for Sample 1–9.50 nm, for Sample 2–10.72 nm, respectively (Table 4). However, the structure of Sample 2 is well described using the t-plot analysis: the calculated specific surface area of micropores (S_{micro}) was 18.32 m^2/g, and the external surface ($S_{external}$)—185.23 m^2/g, which is in agreement with $S_{BET} = 203.55$ m^2/g. At the same time, the micropore volume (V_{micro}) is insignificant and is only 0.006 cm^3/g at a total pore volume of about 0.4 cm^3/g (Table 4). Taking into account the features of the isotherm, the hysteresis shape and the average pore diameter value, it can be concluded that the sample is mainly macroporous with micropores in the walls of the slit-like pores.

The isotherm for Sample 3 can be considered as the Type II - isotherm with completely reversible desorption, or as Type 4 with a very narrow hysteresis in the range of high values of relative pressures of Type H-3. In either case, the narrow hysteresis loop or complete reversibility of the desorption-adsorption isotherm is the first condition to be satisfied for "normal" monolayer-multilayer adsorption on an open and stable surface. The narrow hysteresis loop can be a result of inter-particles capillary condensation usually within non rigid aggregates. Such type of ads-des process which allows unrestricted multimolecular adsorption to occur at high p/p_0 is more usual for non-porous or macroporous materials. At the same time the Type H-3 loops are often given by aggregates of platy particles giving rise to slit-shaped pores (Sing 1994). The uptake at Point B – the beginning of the middle quasi linear section – is usually considered to represent the completion of the monolayer (monolayer capacity) (MC), for Sample 3 it is 24.42 cm^3/g and observed at $p/p_0 = 0.08$ - at the same p/p_0 as for Sample 1 with MC = 110.21 cm^3/g (Fig. 4,a). The intercept of the t-plot appears on the negative side of the scale that points out of the absence of micropore as for Sample 1. The middle pore size is twice larger than for Sample 1- $D_{BJH} = 18.71$ nm—but the specific surface area is less than four times ($S_{BET} = 112.01$ m^2/g, $S_{BJH} = 119.91$ m^2/g). The Cumulative Pore Area as well as Pore Size Distribution curve do not have evident extrema except for a weakly expressed broad peak at 9.4 nm (A = 88 cm^2/g). At a relatively low specific surface area but smaller than Samples 1 and 2—the volume of pores V_{BJH} is 0.561 cm^3/g which is larger than for the sample with slit-shaped macropores and micropores in the pore walls (Sample 2, $V_{BJH} = 0.358$ cm^3/g). Summing up, it can be assumed that Sample 3 is the powder with laminated structure aggregates with an accessible surface of both the external and the slit-shaped open pores.

3.4 Morphology of PSM-DVB, DMSPS-DVB, and BES. DM-DVB microspheres

In Fig. 5 the real shapes of the PSM-DVB, DMSPS-DVB, and BES.DM-DVB microspheres are presented. The photos were made using an optical microscope. The photographs (Fig. 5) clearly show that the resulting microspheres possess a regular spherical morphology and uniform size, and they have a tendency to agglomerate. The DMSPS-DVB microspheres have the smallest particle size, with the diameters in the range of 15–50 μm. The BES.DM-DVB microspheres possess the most uniform spherical shape and a more homogeneous size distribution. These particles have diameters in the range of 30–100 μm.

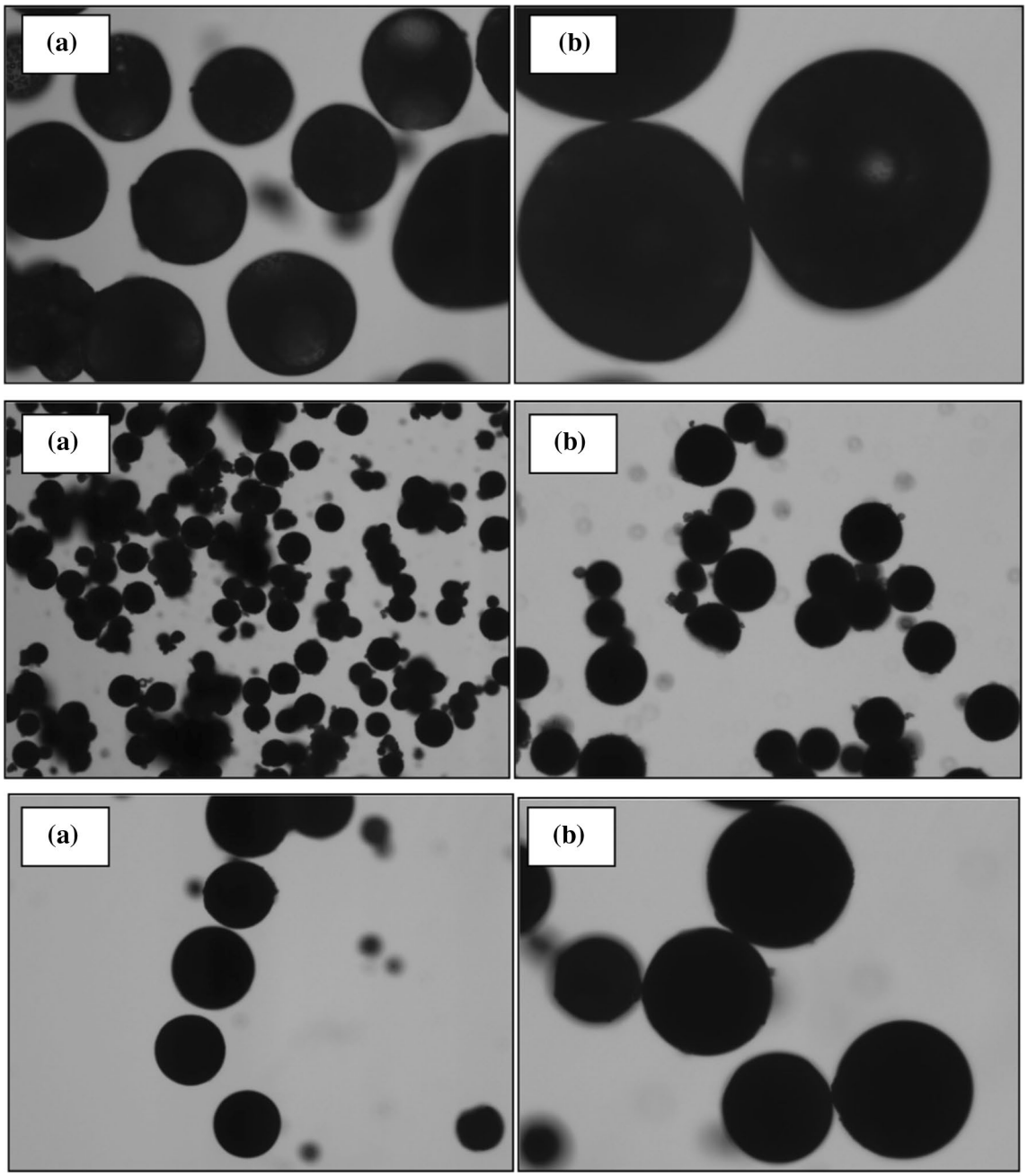

Fig. 5 Optical images of the PSM-DVB (1), DMSPS-DVB (2), and BES.DM-DVB (3) copolymers (**a** 100 µm, **b** 50 µm)

3.5 Swelling studies

Swellability is the main factor that determines access to the internal functional group. The ability to swell causes increase in the volume of polymer beads and network flexibility. Figure 6 presents the swelling properties of the studied microspheres. The results of swellability coefficients for the obtained copolymers beads vary from 0 to 122%. Their largest values are observed for the PSM-DVB microspheres in all organic solvents, such as: acetone (122%), chloroform (122%), THF (113%), acetonitrile (111%), toluene (110%), and methanol (100%). The obtained microspheres do not swell in distilled water. The smallest tendencies to swell for the DMSPS-DVB microspheres were observed. These results show that larger swelling takes place when the polymer network can interact with the solvents containing suitable polar groups.

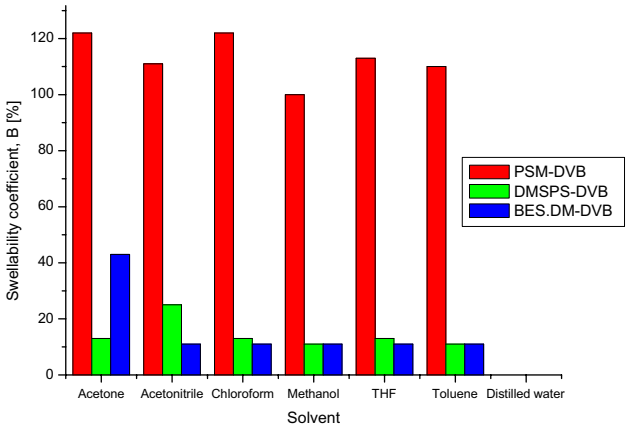

Fig. 6 Swellability coefficients for the PSM-DVB, DMSPS-DVB, and BES.DM-DVB microspheres

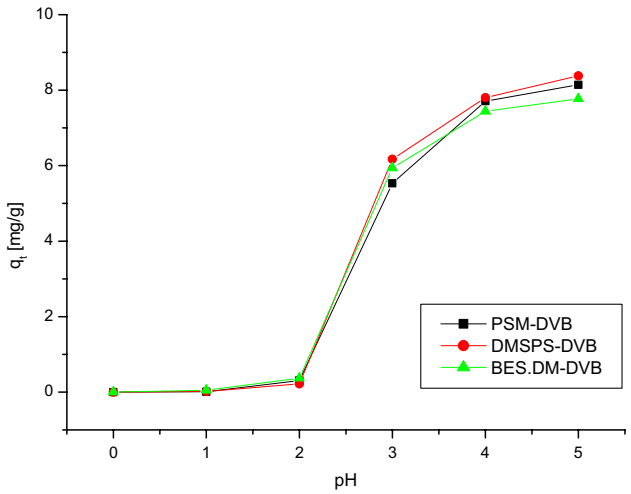

Fig. 7 Effect of pH on the adsorption process of Pb(II) ions

Table 5 The sulfur content in the tested microspheres

Sample	Sulfur content, % mass	
	Experimental value	Theoretical value
PSM-DVB	1.16 ± 0.04	10.39
DMSPS-DVB	14.7 ± 0.4	17.65
BES.DM-DVB	4.85 ± 0.15	5.06

3.6 WD-XRF analysis

Table 5 shows the results from the WD-XRF analysis. This confirms the presence of sulfur in the obtained microspheres (PSM-DVB, DMSPS-DVB, and BES.DM-DVB). The highest content of sulfur is found in the DMSPS-DVB microspheres (approximately 14.7% of the total mass of polymer), while the smallest amount of sulfur is observed in the PSM-DVB microspheres (about 1.2% of the total mass of polymer). Comparing experimental and theoretical values of sulfur content, it can be concluded that the best agreement was obtained for the DMSPS-DVB and BES.DM-DVB microspheres (Table 5). In the case of PSM-DVB microspheres, the experimental value of sulfur content deviates significantly from the theoretical value, which may be caused by incomplete incorporation of sulfur monomer into the polymer structure during synthesis.

3.7 Evaluation of sorption properties

3.7.1 Effect of pH

Standard solutions with an initial concentration of 50 mg/L for Pb(II) ions, fixed quantity of adsorbent, fixed time, and fixed temperature were used. The pH of the solutions was adjusted to five different pH values, namely 1, 2, 3, 4, and 5, using 0.1 mol/L sodium hydroxide and 0.1 mol/L hydrochloric acid. Measurements at pH 6 (and higher) were not made because lead hydroxide precipitated under these conditions. Figure 7 shows adsorption at different pH values. The amount of adsorbed Pb(II) increased with the increasing pH from 2 to 5. As a result, uptake of metal ions increases with the increasing pH value. For all adsorbents the maximum sorption capacities were found at pH = 5. The sorption efficiency for Pb(II) ions on the PSM-DVB, DMSPS-DVB, and BES.DM-DVB microspheres ranged from 82 to 86%. The results of effectiveness of lead ions removal for the three tested adsorbents are presented in Table 6.

Table 6 The effectiveness of lead ions removal depending on the pH for the three tested adsorbents

Sample	pH	q_t (mg/g)	%S
PSM-DVB	1	0.01	0.1
	2	0.31	3.2
	3	5.53	57.2
	4	7.71	82.4
	5	8.14	86.1
DMSPS-DVB	1	0.02	0.2
	2	0.22	2.3
	3	6.17	63.9
	4	7.80	83.3
	5	8.38	88.7
BES.DM-DVB	1	0.05	0.5
	2	0.37	3.9
	3	5.94	61.5
	4	7.44	79.4
	5	7.77	82.2

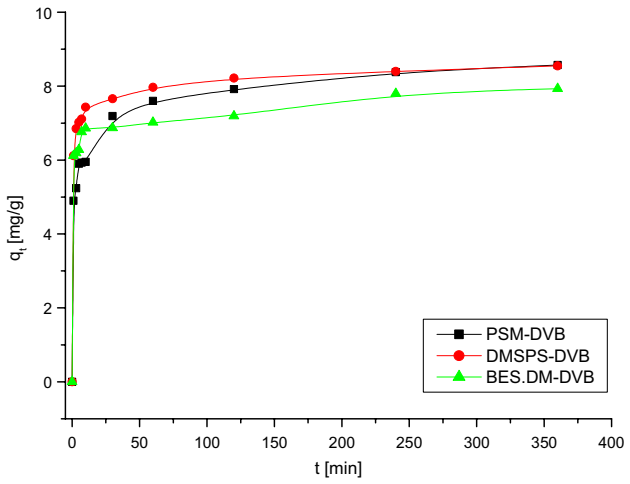

Fig. 8 Effect of contact time on the adsorption process of Pb(II) ions

3.7.2 Effect of contact time

The experimental studies on the effect of contact time on the adsorption of Pb(II) ions were carried out at various time intervals from 1 to 360 min and at room temperature, pH 5, the initial concentration 50 mg/L for Pb(II) ions, and an adsorbent mass of 0.05 g, to obtain the optimal time required for adsorption. The concentrations of Pb(II) ions were determined at the end of each period of time. Figure 8 shows the effect of contact time on Pb(II) ions adsorption.

The amount of adsorbed Pb(II) ions increased rapidly with an increase in the phase contact time. The adsorption equilibrium was reached after 240 min. A further increase in time had no effect on the adsorption. Therefore, the maximum contact time of 240 min was considered as the optimum time for adsorption. For Pb(II) ions the sorption efficiency of the studied microspheres varied from 54 to 95%. The highest sorption capacity was achieved by the PSM-DVB microspheres.

3.7.3 Adsorption kinetics and isotherm studies

To determine the adsorption kinetics of Pb(II) ions on PSM-DVB, DMSPS-DVB, and BES.DM-DVB microspheres, the pseudo-first order, pseudo-second order, and intraparticle diffusion kinetic models were used. Table 7 shows the calculated parameters of these models. Comparing the obtained values of determination coefficients R^2, it can be seen that the adsorption process on these materials is best described by the pseudo-second order model. The R^2 values equal to 0.999 were obtained. However, the pseudo-first and pseudo-second order models do not describe the process mechanism. To describe the mechanism of adsorption process the Weber Morris intraparticle diffusion model was used. The parameters of this model were calculated from the plot q_t vs. $t^{1/2}$. The intraparticle diffusion is the rate limiting step in the adsorption if this plot gives a straight line. Based on the results, it was found that the curve does not pass through indicating that intraparticle diffusion is not the only step limiting the adsorption rate. The constant C in this model means the thickness of boundary layer. The higher the C value, the greater the effect of the diffusion layer on the adsorption process. The highest C value was obtained for the PSM-DVB microspheres.

The effect of the initial concentrations of Pb(II) ions on the sorption capacity of PSM-DVB, DMSPS-DVB, and BES.DM-DVB microspheres was also investigated. The results show that when the initial Pb(II) ions concentration increases from 25 mg/L to 500 mg/L, Pb(II) adsorption increases from 2 to 20.5 mg/g. Various adsorption isotherm models, such as the Langmuir and Freundlich ones were

Table 7 Kinetic parameters for the adsorption of Pb(II) ions on PSM-DVB, DMSPS-DVB, and BES.DM-DVB (C_0 = 50 mg/L, m = 0.05 g, V = 10 mL, T = 293 K)

Sample	q_{exp}	Pseudo-first order			Pseudo-second order			Intraparticle diffusion model		
		q_1	k_1	R^2	q_2	k_2	R^2	k_i	C	R^2
PSM-DVB	8.55	1.51	0.011	0.912	8.54	0.056	0.999	0.176	6.53	0.817
DMSPS-DVB	8.57	2.79	0.012	0.949	8.58	0.027	0.999	0.198	5.39	0.865
BES.DM-DVB	7.93	1.58	0.010	0.924	7.92	0.039	0.999	0.101	6.22	0.728

Table 8 Isotherm parameters for the adsorption of Pb(II) ions on PSM-DVB, DMSPS-DVB, and BES.DM-DVB

Sample	Langmuir				Freundlich		
	q_0		K_L (L/mg)	R^2	n	K_F (mg/g)	R^2
	mg/g	mmol/g					
PSM-DVB	21.43	0.1035	0.038	0.995	2.492	2.33	0.941
DMSPS-DVB	22.54	0.1089	0.024	0.997	2.049	1.46	0.923
BES.DM-DVB	20.80	0.1005	0.074	0.998	3.041	3.61	0.908

commonly used to describe the adsorption characteristics of the sorbents. The adsorption isotherm parameters of Pb(II) on PSM-DVB, DMSPS-DVB, and BES.DM-DVB were obtained by studying the relationship C_e versus q_e. The calculated parameters are shown in Table 8. On the basis of the determination coefficient values, R^2, it was found that the adsorption process proceeds according to the Langmuir model. The Langmuir model assumes that there is a monolayer coverage of the adsorbent surface with Pb(II) ions. The Langmuir adsorption constants q_0 and K_L are related to the adsorption capacity and the energy of adsorption, respectively. The highest value q_0 was obtained for DMSPS-DVB. The Freundlich model is applied to non-ideal sorption on heterogeneous surfaces as well as multilayer adsorption. For this model lower values of R^2 were obtained. The value of K_F is related to the adsorption capacity of the PSM-DVB, DMSPS-DVB, and BES.DM-DVB microspheres. The higher the K_F value, the higher affinity of the Pb(II) ions for the adsorbent. The greatest K_F value was obtained for the BES.DM-DVB adsorbent. The values of n from 1 to 10 indicate favourable adsorption (Podkościelna 2013). Figure 9 compares the fit of experimental data with data obtained from the Langmuir and Freundlich isotherms. As it can be seen, the best fit was received for the Langmuir isotherm.

3.7.4 Adsorption mechanism

Li et al. (2018) synthesized the poly(2,5-dimercapto-1,3,4-thiadiazole) (PBT) nanosheets by using a chemical oxidative polymerization of 2,5-dimercapto-1,3,4-thiadiazole (BT) monomer. They investigated that the PBT nanosheets can be excellent adsorbents for mercury ions, with an adsorption capacity as high as 680.01 mg/g and a very rapid initial adsorption rate of up to 10.653 mg/gh. It has been previously reported that BT and its derivatives demonstrate strong abilities for heavy metal ions coordination (Tzvetkova et al. 2010; Jing et al. 2009) because of the sulfur (S)- and nitrogen (N)-rich subgroups and their extremely high total molar content (56%) in the BT molecules. Hence, BT can be used for effective coordination of a variety of heavy metal ions to form the BT-M^{n+} (2:1) metal coordination polymer (El-Shekeil et al. 2007; Tiwari et al. 2014), depending on the strong coordination ability of electron-rich nitrogen and sulfur subgroups.

According to Pearson, in the acid–base reactions hard acids prefer to interact with hard bases, and soft acids with soft bases. (Being soft bases, sulfur sites should have greater affinity for soft acids such as Hg(II) or Pb(II) and smaller affinity for borderline acids like Cu(II) or Ni(II)). Probably the S sites are more accessible to sorption than oxygen ones which may be protonized (Tzvetkova et al. 2010; Pearson 1963; Jing et al. 2009).

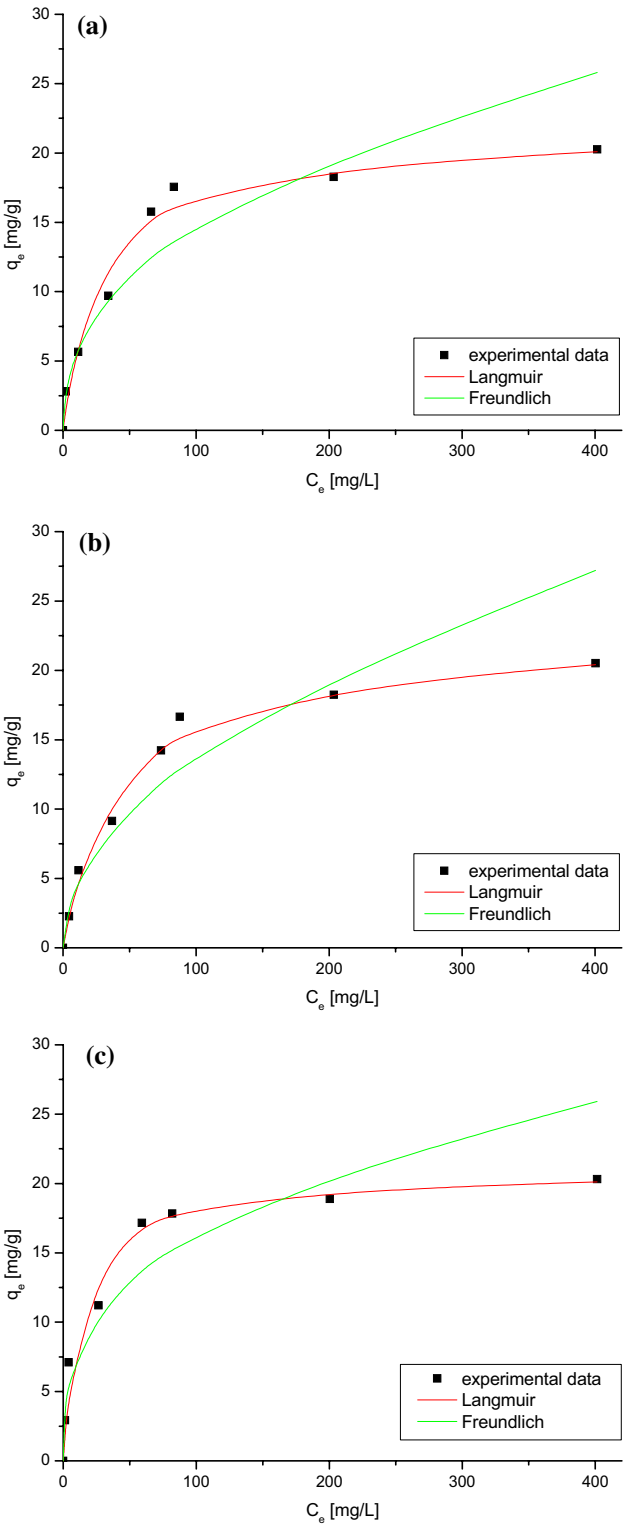

Fig. 9 Fitting of used isotherms to the experimental data for sorption of Pb(II) ions for the PSM-DVB (**a**), DMSPS-DVB (**b**), and BES.DM-DVB (**c**) microspheres

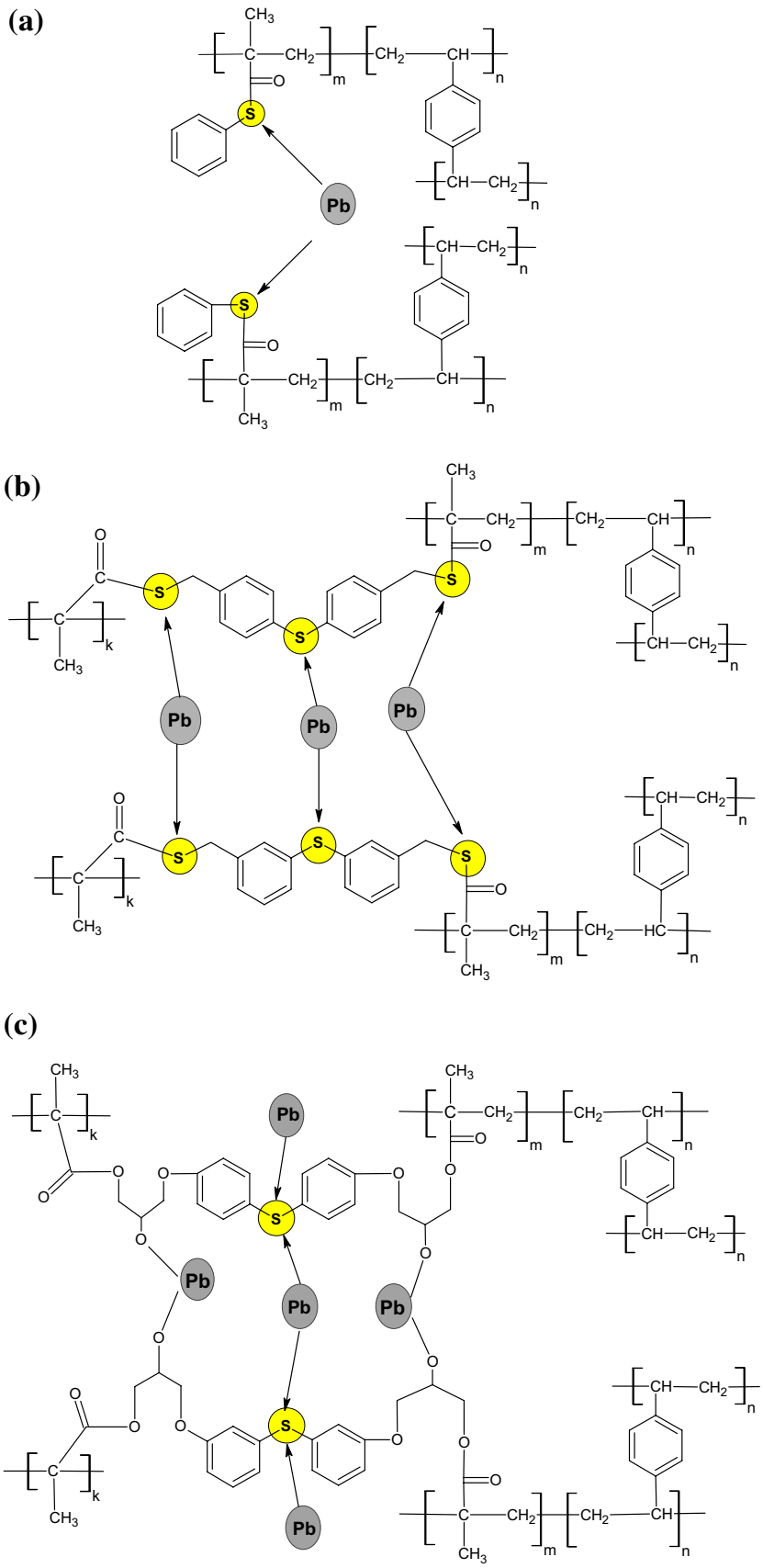

Fig. 10 Proposed adsorption mechanism of Pb(II) ions on (**a**) PSM-DVB, (**b**) DMSPS-DVB, and (**c**) BES.DM-DVB microspheres

Based on the above studies, the proposed adsorption mechanism of the obtained microspheres for Pb(II) is presented in Fig. 10. Due to the presence of sulfur in the structure of the PSM-DVB, DMSPS-DVB, and BES.DM-DVB microspheres, coordination bonds can appear between sulfur atoms and heavy metal ions, in this case—S-Pb, not discarding the possibility of the existence of protonated sulfur atoms. Since the aqueous solution of the adsorbate $Pb(NO_3)_2$ is acidic, the electron-donating sulfur atoms are readily bound to H^+ ions to form S–H bonds. After all, the formation of S–Pb coordination bonds suggests that sulfur atoms are the active sites of lead ions adsorption. Additionally, in the BES.DM-DVB microspheres, bonds between oxygen and lead ions (O–Pb) are likely to appear. The suggested mechanism was confirmed by comparing the maximum adsorbed amount of lead (in mmol/g from Langmuir equation) (Table 8) with content of sulfur in the polymers (Table 5). According to this mechanism, theoretically PSM-DVB and DMSPS-DVB microspheres should bind lead as S:Pb ratio equal to 1:1, while for BES.DM-DVB microspheres—S:Pb it should be 1:2. Analysis of experimental results confirms agreement for the assumed mechanisms for DMSPS-DVB and BES.DM-DVB microspheres. In the case of PSM-DVB microspheres, the experimental sulfur content is not consistent with the theoretical value and this is due to the small amount of sulfur monomer present in the polymer structure of which the main part is DVB.

4 Conclusions

The synthesis of the new aromatic methacrylate microspheres of derivatives of three aromatic thiols: S-phenyl 2-methylprop-2-enethioate (PSM), S,S′-thiodi-4,1-phenylenebis(thiomethacrylate) (DMSPS), and bis[4(2-hydroxy-3-methacryloyloxypropoxy)phenyl]sulfide (BES.DM) with divinylbenzene (DVB) was presented. In the presence of pore-forming diluents mixture (toluene and decan-1-ol), highly crosslinked porous microspheres were obtained. Porous structures of the obtained microspheres were studied in detail. A detailed spectroscopic analysis (ATR/FT-IR) of the resulting compounds was made which allowed to determine their chemical structures. The materials obtained by copolymerization have a very good thermal resistance. The results of the DSC analysis indicate one endothermic effect (in the range 372–441 °C) due to the total decomposition of the copolymers. The swellability coefficients for the PSM-DVB copolymer are the highest of the studied compounds. The smallest values of this coefficient for the DMSPS-DVB microspheres are observed. The WD-XRF analysis confirmed the presence of sulfur in the synthesized microspheres. The sorption process of Pb(II) ions on the PSM-DVB, DMSPS-DVB, and BES.DM-DVB microspheres depends on experimental conditions. The sorption medium pH, contact time, and the initial concentration of heavy metal ions had significant effects on the sorption capacity. The sorption kinetics is well described by the pseudo-second order model. The sorption process is best described by the Langmuir isotherm model. The PSM-DVB, DMSPS-DVB, and BES.DM-DVB microspheres were successfully used as adsorbing materials for removal of Pb(II) ions from aqueous solutions due to the well-developed surface area and the presence of mesopores.

Acknowledgements The research leading to these results has received funding from the People Programme (Marie Curie Actions) of the European Union's Seventh Framework Programme FP7/2007–2013/ under REA grant agreement no PIRSES-GA-2013-612484. The authors are grateful for the collaboration with Prof. D. Kołodyńska and Mgr D. Fila and for their valuable support during the experimental part based on sorption tests.

References

Amin, M.M., Khodabakhsi, A.: Removal of Cr(VI) from simulated electroplating wastewater by magnetite nanoparticles. Environ. Eng. Manag. J. **9**, 921–927 (2010)

Carlos, L., Einschlag, F.: Waste water-treatment technologies and recent analytical developments, Chap. 3: Applications of Magnetite Nanoparticles for Heavy Metal Removal from Wastewater, pp. 63–77. InTech: (2013)

Condon, J.B.: Surface, Area and Porosity Determinations by Physisorption, Measurements and Theory. Elsevier, Amsterdam (2006)

Donohue, M.D., Aranovich, G.L.: Adsorption hysteresis in porous solids. J. Colloid Interface Sci. **205**, 121–130 (1998a)

Donohue, M.D., Aranovich, G.L.: Classification of Gibbs adsorption isotherms. Adv. Colloid. Interface Sci. **76–77**, 37–152 (1998b)

El-Shekeil, A.G., Al-Maydama, H.M., Al-Shuja'a, O.M.: The synthesis, characterization, and DC electrical conductivity of poly[di(2,5-dimercapto-1,3,4-thiadiazole)-metal] complexes. J. Appl. Polym. Sci. **106**, 2427–2435 (2007)

Fila, K., Grochowicz, M., Podkościelna, B.: Thermal and spectral analysis of copolymers with sulfur groups. J. Therm. Anal. Calorim. **133**, 489–497 (2018)

Freundlich, H.F.M.: Über die adsorption in lösungen. Z. Phys. Chem. **57**, 385–470 (1906)

Giraldo, J., Erto, A., Moreno-Pirajan, J.C.: Magnetite nanoparticles for removal of heavy metals from aqueous solutions: synthesis and characterization. Adsorption **19**, 465–474 (2013)

Goon, I.Y., Zhang, C., Lim, M., Gooding, J.J., Amal, R.: Controlled fabrication of polyethyl-enimine-functionalized magnetic nanoparticles for the sequestration and quantification of free Cu^{2+}. Langmuir **26**, 12247–12252 (2010)

Gregg, S.J., Sing, K.S.W.: Adsorption, Surface Area and Porosity, 2nd edn. Academic Press, London (1991)

Grochowicz, M., Gawdzik, B.: Preparation and characterization of porous crosslinked microspheres of new aromatic methacrylates. J. Porous. Mater. **20**, 339–349 (2013)

Hao, J., Han, M., Meng, X.: Preparation and evaluation of thiol-functionalized activated alumina for arsenite removal from water. J. Hazard. Mater. **167**, 1215–1221 (2009)

He, F., Wang, W., Moon, J., Howe, J., Pierce, E.M., Liang, L.: Rapid removal of Hg(II) from aqueous solutions using thiol-functionalized Zn-doped biomagnetite particles. ACS Appl. Mater. Interfaces **4**, 4373–4379 (2012)

Ho, T.L.: Hard soft acids bases (HSAB) principle and organic chemistry. Chem. Rev. **75**, 1–20 (1975)

Hua, M., Zhang, S., Pan, B.: Heavy metal removal from water/wastewater by nanosized metal oxides: a review. J. Hazard. Mater. **211–212**, 317–331 (2012)

Huang, M.R., Huang, S.J., Li, X.G.: Facile synthesis of polysulfoaminoanthraquinone nanosorbents for rapid removal and ultrasensitive fluorescent detection of heavy metal ions. J. PhysChem. C **115**, 5301–5315 (2011)

Jing, X.S., Liu, F.Q., Yang, X., Ling, P.P., Li, L.J., Long, C., Li, A.M.: Adsorption performances and mechanisms of the newly synthesized N,N′-di (carboxymethyl) dithiocarbamate chelating resin toward divalent heavy metal ions from aqueous media. J. Hazard. Mater. **167**, 589–596 (2009)

Kesenci, K., Tuncel, A., Pişkin, E.: Swellable ethylene glycol dimethacrylate-hydroxyethyl methacrylate copolymer beads. React. Funct. Polym. **31**, 137–147 (1996)

Langmuir, I.: The constitution and fundamental properties of solids and liquids. J. Am. Chem. Soc. **38**, 2221–2295 (1916)

Lee, C.H., Chiang, C.L., Liu, S.J.: Electrospun nanofibrous rhodanine/polymethylmethacrylate membranes for the removal of heavy metal ions. Sep. Purif. Technol. **118**, 737–743 (2013)

Li, G., Zhao, Z., Liu, J., Jiang, G.: Effective heavy metal removal from aqueous systems by thiol functionalized magnetic mesoporous silica. J. Hazard. Mater. **192**, 277–283 (2011)

Li, C., Huang, S., Min, C., Du, P., Xia, Y., Yang, C., Huang, Q.: Highly productive synthesis, characterization and fluorescence and heavy metal ion adsorption properties of poly(2,5-dimercapto-1,3,4-thiadiazole) nanosheets. Polymers **10**, 24–50 (2018)

Liu, J.F., Zhao, S.Z., Jiang, G.B.: Coating Fe_3O_4 magnetite nanoparticles with humic acid for high efficient removal of heavy metals in water. Environ. Sci. Technol. **42**, 6949–6954 (2008)

Neyaz, N., Siddiqui, W.A., Nair, K.K.: Application of surface functionalized iron oxide nanomaterials as a nanosorbents in extraction of toxic heavy metals from ground water: A review. Int. J. Environ. Sci. **4**, 472–483 (2013)

Pan, B., Pan, B., Zhang, W., Lv, L., Zhang, Q.: Development of polymeric and polymer-based hybrid adsorbents for pollutants removal from waters. Chem. Eng. J. **151**, 19–29 (2009)

Pearson, R.: Hard and soft acids and bases. J. Am. Chem. Soc. **85**, 3533–3539 (1963)

Petcharoen, K., Sirivat, A.: Synthesis and characterization of magnetite nanoparticles via the chemical co-precipitation method. Mater. Sci. Eng. B. **177**, 421–427 (2012)

Podkościelna, B.: The use of Bis[4(2-hydroxy-3-methacryloyloxypropoxy) phenyl]sulfide in preparation of microspheres with pendant amine groups as a heavy metal sorbent. Sep. Sci. Technol. **48**, 1699–1708 (2013)

Podkościelna, B., Kołodyńska, D.: A new type of cation-exchange polymeric microspheres with pendant methylenethiol groups. Polym. Adv. Technol. **24**, 866–872 (2013)

Podkościelna, B., Bartnicki, A., Gawdzik, B.: Porous microspheres, copolymers of Bis[4-(2-hydroxy-3-methacryloyloxypropoxy)phenyl]sulfide, and divinylbenzene as stationary phase for HPLC. J. Appl. Polym. Sci. **111**, 1257–1267 (2009)

Podkościelna, B., Kołodyńska, D., Hubicki, Z., Gawdzik, B., Bartnicki, A.: Synthesis, characterization, and application of a new methylenethiol resins for heavy metal ions removal. Sep. Sci. Technol. **51**, 2501–2510 (2016)

Rouquerol, F., Rouquerol, J., Sing, K.: Adsorption by Powders and Porous Solids Principles, Methodology and Applications. Academic Press, San Diego (1999)

Sangwichien, C., Aranovich, G.L., Donohue, M.D.: Density functional theory predictions of adsorption isotherms with hysteresis loops. Colloids Surf. B **206**, 313–320 (2002)

Savage, N., Diallo, M.: Nanomaterials and water purification: opportunities and challenges. J. Nanopart. Res. **7**, 331–342 (2005)

Sing, K.S.W.: Reporting physisorption data for gas/solid systems with special reference to the determination of surface area and porosity. Pure Appl. Chem. **54**, 2201–2218 (1982)

Sing, K.S.W.: Physisorption of gases by carbon blacks. Carbon **32**, 1311–1317 (1994)

Thommes, M., Kaneko, K., Neimark, A.V., Olivier, J.P., Rodriguez-Reinoso, F., Rouquerol, J., Sing, K.S.W.: Physisorption of gases, with special reference to the evaluation of surface area and pore size distribution (IUPAC Technical Report). Pure Appl. Chem. **87**, 1051–1069 (2015)

Tiwari, M., Gupta, S., Prakash, R.: One pot synthesis of coordination polymer 2,5-dimercapto-1,3,4-thiadiazole-gold and its application in voltammetric sensing of resorcinol. RSC Adv. **4**, 25675–25682 (2014)

Tuncel, A., Ecevit, K., Kesenci, K., Pişkin, E.: Nonswellable and swellable ethylene glycol dimethacrylate-acrylic acid copolymer microspheres. J. Polym. Sci. A **34**, 45–55 (1996)

Tzvetkova, P., Vassileva, P., Nickolov, R.: Modified silica gel with 5-amino-1,3,4-thiadiazole-2-thiol for heavy metal ions removal. J. Porous. Mater. **17**, 459–463 (2010)

Yantasee, W., Warner, C., Sangvanich, T., Addleman, R.S., Carter, T., Wiacek, R., Fryxell, G., Timchalk, C., Warner, M.: Removal of heavy metals from aqueous systems with thiol functionalized superparamagnetic nanoparticles. Environ. Sci. Technol. **41**, 5114–5119 (2007)

Zhang, C., Sui, J., Li, J., Tang, Y., Cai, W.: Efficient removal of heavy metal ions by thiol-functionalized superparamagnetic carbon nanotubes. Chem. Eng. J. **210**, 45–52 (2012)

Zhao, X., Lv, L., Pan, B., Zhang, W., Zhang, S.: Polymer-supported nanocomposites for environmental application: a review. Chem. Eng. J. **170**, 381–394 (2011)